Uncertainties of optical parameters and their propagations in an analytical ocean color inversion algorithm

Article *in* Applied Optics · January 2010

DOI: 10.1364/AO.49.000369 · Source: PubMed

CITATIONS
123

READS
176

5 authors, including:

Zhongping Lee
University of Massachusetts Boston
150 PUBLICATIONS **5,691** CITATIONS
SEE PROFILE

Robert Arnone
University of Southern Mississippi
277 PUBLICATIONS **5,614** CITATIONS
SEE PROFILE

Jeremy Werdell
NASA
113 PUBLICATIONS **4,619** CITATIONS
SEE PROFILE

Bertrand Lubac
Université Bordeaux 1
39 PUBLICATIONS **745** CITATIONS
SEE PROFILE

Uncertainties of optical parameters and their propagations in an analytical ocean color inversion algorithm

ZhongPing Lee,[1,*] Robert Arnone,[2] Chuanmin Hu,[3] P. Jeremy Werdell,[4] and Bertrand Lubac[1,2]

[1]Northern Gulf Institute, Mississippi State University, Stennis Space Center, Mississippi 39529, USA

[2]Naval Research Laboratory, Stennis Space Center, Mississippi 39529, USA

[3]College of Marine Science, University of South Florida, St. Petersburg, Florida 33701, USA

[4]NASA Goddard Space Flight Center, Greenbelt, Maryland, 20771, USA

*Corresponding author: zplee@ngi.msstate.edu

Received 16 July 2009; revised 30 October 2009; accepted 24 November 2009; posted 14 December 2009 (Doc. ID 114332); published 13 January 2010

Following the theory of error propagation, we developed analytical functions to illustrate and evaluate the uncertainties of inherent optical properties (IOPs) derived by the quasi-analytical algorithm (QAA). In particular, we evaluated the effects of uncertainties of these optical parameters on the inverted IOPs: the absorption coefficient at the reference wavelength, the extrapolation of particle backscattering coefficient, and the spectral ratios of absorption coefficients of phytoplankton and detritus/gelbstoff, respectively. With a systematically simulated data set (46,200 points), we found that the relative uncertainty of QAA-derived total absorption coefficients in the blue-green wavelengths is generally within $\pm 10\%$ for oceanic waters. The results of this study not only establish theoretical bases to evaluate and understand the effects of the various variables on IOPs derived from remote-sensing reflectance, but also lay the groundwork to analytically estimate uncertainties of these IOPs for each pixel. These are required and important steps for the generation of quality maps of IOP products derived from satellite ocean color remote sensing.

OCIS codes: 010.4450, 280.4991.

1. Introduction

To describe, understand, and forecast the interactions and changes associated with environments and climate, it is critical to have reliable long-term observations of geophysical properties for the atmosphere as well as for the land and oceans. For such a daunting requirement, measurements by satellite remote sensors are indispensable. To meet this requirement, systematic observations of the biogeochemical properties of global oceans through the measurement of ocean color (ocean color radiometry—OCR) from space have become an important component of the Earth Observing System [1], and various ocean color missions, such as the CZCS (Coastal Zone Color Scanner, 1978–1986), SeaWiFS (Sea-viewing Wide Field-of-view Sensor, 1997–present), MODIS (Moderate Resolution Imaging Spectroradiometer, 1999–present), and MERIS (Medium Resolution Imaging Spectrometer, 2002–present) instruments that have been launched since the late 1970s [2].

The derived products from OCR generally include inherent optical properties (IOPs; e.g., marine absorption and scattering coefficients), concentrations of chlorophyll-a and suspended matters, and water clarity [3]. These products, however, inherently contain some degree of uncertainty because of imperfect

0003-6935/10/030369-13$15.00/0

sensor engineering and retrieval algorithms [4–7]. Conventionally, such uncertainties, sometimes called "errors," are evaluated statistically by comparing retrieved values from remote sensing with those from water samples of concurrent measurements, and an *averaged* uncertainty for the entire data set [8], or subgroups [9], is usually obtained. This quantity provides a general picture about the consistency between retrieved and measured properties. By the nature of the evaluation method, however, this quantity, especially the *averaged* "error" derived from a data set covering a wide dynamic range, does not represent the uncertainty for a particular pixel in satellite imagery. Also note that this quantity does not necessarily represent algorithm or satellite retrieval error, as errors associated with various *in situ* or lab measurements are not removed in the comparison.

At present, there is no quantitative measure able to describe the quality (or uncertainty) of satellite products pixelwise, although eight quality levels of chlorophyll-*a* concentration could be obtained based on the class-based approach recently developed by Moore *et al.* [9]. Consequently, this limits the uncertainty evaluation of next level products, such as primary production [10,11] or water quality [12–14] and prevents a full account of errors or uncertainties in closure analyses [15] or trend evaluations [16].

Note that satellite ocean color remote sensing is a complex system with many variables and steps involved before bio-optical products are finally generated. Major variables/steps include, in a sequential order, sensor calibration [17], atmospheric correction [18], and inversion of optical and biogeochemical properties [8,19] from the spectrum of water-leaving radiance (or remote sensing reflectance). Each variable/step has its own sources and levels of uncertainties; thus it is required to understand the sources of uncertainties and quantify the quality of the products of each step [6].

For the bio-optical inversion, Wang *et al.* [20] proposed a scheme to obtain ensembles of solutions for each spectral remote sensing reflectance spectrum (r_{rs}, in units Sr^{-1}, representing subsurface remote-sensing reflectance, which can be derived from above-surface remote-sensing reflectance, R_{rs}, after correcting the air–sea surface effects [21]) via a linear matrix inversion method [22]. Depending on the setup of the ranges and steps of the spectral shapes of the major components, such an approach could result in more than 1000 combinations of inversions to be carried out for each r_{rs} spectrum [20]. This computational requirement makes it rather difficult to be incorporated into operational processing where large quantities of satellite images have to be processed.

The quasi-analytical algorithm (QAA) [13,23], on the other hand, derives IOPs from r_{rs} in a stepwise fashion with every variable also explicitly described. This characteristic makes it easy to propagate and evaluate the effects of uncertainties of each variable based on the theory of error propagation [24]. To highlight this feature and to evaluate the uncertainties introduced by QAA, we developed analytical expressions to describe the uncertainties of optical variables and their propagations in the QAA process (see Fig. 1 for a schematic flowchart of the steps and the variables whose uncertainties are evaluated and propagated). In particular we evaluated the uncertainty and propagation of the following: the absorption coefficient at the reference wavelength, the extrapolation of particle backscattering coefficient from one wavelength to another (represented by a power coefficient), and the spectral ratios of absorption coefficients of phytoplankton and detritus/gelbstoff, respectively. The results of this study provide important components that are required for the generation of quality maps of IOPs products.

2. Overview of Quasi-Analytical Algorithm and Uncertainty Propagation

A. Quasi-Analytical Algorithm Overview

QAA is an inversion algorithm [23] that derives water's IOPs from a spectral r_{rs}, as IOPs provide the key connection between in-water constituents and spectral radiance from a water body [25,26]. The following equations provide a concise summary of QAA steps and data flow.

The quantity u is defined as

$$u(\lambda) = \frac{b_b(\lambda)}{a(\lambda) + b_b(\lambda)}. \tag{1}$$

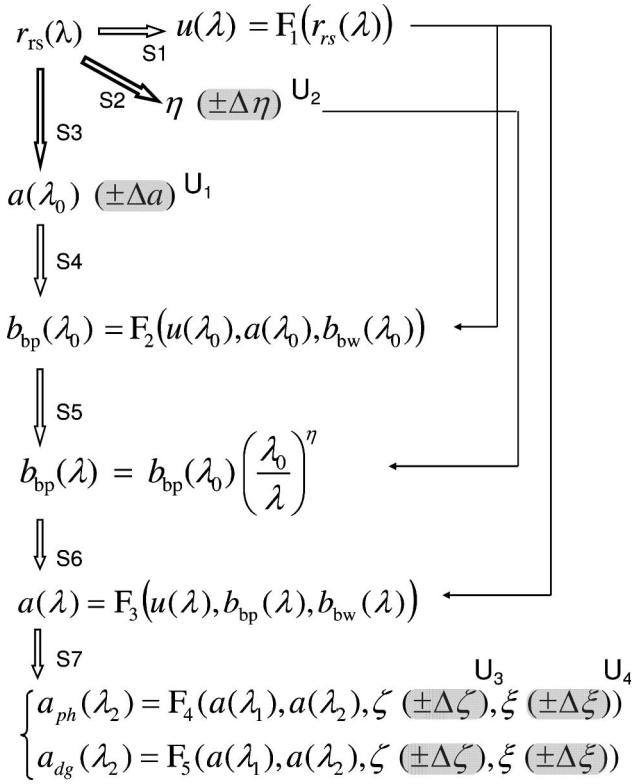

Fig. 1. Schematic chart to show variables and steps (S1–S7) involved in the QAA procedure, redrawn from Lee *et al.* [23]. Variables with uncertainties (U_1–U_4) discussed in this study are highlighted with gray, while all others assumed error free.

Here b_b and a represent the total backscattering and absorption coefficients (units of m^{-1}), respectively. The symbol λ represents wavelength (units of nm). In the current QAA procedure and other semi-analytical algorithms [22,27,28], u can be derived from measured r_{rs} through a model [29,30]:

$$r_{rs}(\lambda) = (g_0 + g_1\, u(\lambda))u(\lambda). \tag{2}$$

Here g_0 and g_1 are model constants, and their values vary with Sun-sensor angular geometry [31], although they are considered wavelength and water-property independent. Equation (2) is an approximation [32] from the radiative transfer equation, so the expression is not error free. However, because the error in Eq. (2) is significantly less than 10% [29] and this study focuses on the uncertainties specifically introduced by the QAA procedure, the minor uncertainty introduced by Eq. (2) is omitted here.

For convenience in algebraic derivations, quantities A and B are defined, respectively, as

$$A(\lambda) = \frac{1 - u(\lambda)}{u(\lambda)}, \tag{3}$$

$$B(\lambda) = \frac{u(\lambda)}{1 - u(\lambda)}. \tag{4}$$

When the absorption coefficient at a reference wavelength ($\lambda_0 = 555$, 551, or 560 nm for SeaWiFS, MODIS, and MERIS, respectively), $a(\lambda_0)$, is estimated through [13] (also see http://www.ioccg.org/groups/Software_OCA/QAA_v5.pdf for recent updates)

$$\begin{aligned} \chi &= \log\left(\frac{r_{rs}(443) + r_{rs}(490)}{r_{rs}(\lambda_0) + 5\frac{r_{rs}(667)}{r_{rs}(490)} r_{rs}(667)}\right), \\ a(\lambda_0) &= a_w(\lambda_0) + 10^{-1.146 - 1.366\chi - 0.469\chi^2}, \end{aligned} \tag{5}$$

where $a_w(\lambda_0)$ is the contribution of pure water [33]. Then $b_{bp}(\lambda_0)$ is calculated by

$$b_{bp}(\lambda_0) = B(\lambda_0)\, a(\lambda_0) - b_{bw}(\lambda_0). \tag{6}$$

To calculate $a(\lambda)$ requires extrapolation of b_{bp} at λ_0 to λ. The relationship between b_{bp} at two wavelengths can be generally expressed as

$$b_{bp}(\lambda) = b_{bp}(\lambda_0)\, \rho(\lambda, \lambda_0). \tag{7a}$$

For easy extrapolation and following tradition [25,34], $\rho(\lambda, \lambda_0)$ in QAA is modeled as

$$\rho(\lambda, \lambda_0) = \left(\frac{\lambda_0}{\lambda}\right)^{\eta}, \tag{7b}$$

with η estimated from

$$\eta = 2.0\left[1 - 1.2\, \exp\left(-0.9\frac{r_{rs}(440)}{r_{rs}(550)}\right)\right]. \tag{8}$$

The absorption coefficient at λ is then calculated:

$$a(\lambda) = A(\lambda)(b_{bp}(\lambda) + b_{bw}(\lambda)). \tag{9}$$

When $a(\lambda_1)$ and $a(\lambda_2)$ are known, $a_{dg}(\lambda_2)$ and $a_{ph}(\lambda_2)$ are further calculated:

$$\begin{aligned} a_{dg}(\lambda_2) &= \frac{[a(\lambda_1) - \zeta\, a(\lambda_2)] - [a_w(\lambda_1) - \zeta\, a_w(\lambda_2)]}{\xi - \zeta}, \\ a_{ph}(\lambda_2) &= \frac{[\xi a(\lambda_2) - a(\lambda_1)] - [\xi a_w(\lambda_2) - a_w(\lambda_1)]}{\xi - \zeta}. \end{aligned} \tag{10}$$

Here the parameters ζ and ξ represent the ratio of $a_{ph}(\lambda_1)/a_{ph}(\lambda_2)$ and $a_{dg}(\lambda_1)/a_{dg}(\lambda_2)$, respectively. In QAA, the value of ζ is estimated empirically from $r_{rs}(\lambda)$, and ξ is estimated with $\exp[S(\lambda_2 - \lambda_1)]$. Here S (units of nm^{-1}) is the spectral slope of the combined absorption coefficient of gelbstoff and detritus [28]. The wavelengths λ_1 and λ_2 are normally selected as 412 nm and 443 nm, respectively, to reflect spectral configurations of satellite sensors (e.g., SeaWiFS/MODIS). The subscripts w, ph, dg, and p stand for water molecules (including salt effects), phytoplankton, detritus/gelbstoff, and particles, respectively.

B. Uncertainties and Their Propagations

In general, for a variable z that is a function of various independent variables x_i,

$$z = f(x_i, i : 1 \Rightarrow N), \tag{11}$$

the uncertainty of z, Δz, can be expressed as [24,35]

$$\Delta z = \sqrt{\sum_{i=1}^{N} [\Delta z(\Delta x_i)]^2}. \tag{12a}$$

Here $\Delta z(\Delta x_i)$ is the uncertainty in z that results from uncertainty of x_i, Δx_i. This equation is also commonly expressed as [24]

$$\Delta z = \sqrt{\sum_{i=1}^{N} \left(\frac{\partial z}{\partial x_i} \Delta x_i\right)^2}, \tag{12b}$$

with $\partial z/\partial x_i$ a partial derivative of z over x_i.

In the QAA process, the variables $r_{rs}(\lambda)$, $a(\lambda_0)$, $\rho(\lambda, \lambda_0)$ (or η), ζ, and ξ are involved at various steps (see Fig. 1). Although their values may be estimated from the same $r_{rs}(\lambda)$, e.g., $a(\lambda_0)$ or η, there are no observations indicating that their uncertainties covary; therefore the uncertainties of these variables are considered independent of each other. Also, it is necessary to keep in mind that an IOP product is not necessarily affected by all of these variables. For instance, the value of $\rho(\lambda, \lambda_0)$ (or η) has no effect on the estimation of $b_{bp}(\lambda_0)$, and the values of ζ and ξ have no effect on the estimation of $a(\lambda)$. We recognize that r_{rs} from satellite or any platform is not error free

(e.g., Antoine *et al.* [7], Hu *et al.* [36], and Zibordi *et al.* [7,37]), but this measurement-introduced uncertainty is omitted in this study as it is not yet clear about the pixel-specific uncertainty of a measured r_{rs}. The following is thus focused on how the uncertainties of $a(\lambda_0)$, η, ζ, and ξ affect the quality of derived IOPs.

a. Uncertainty in estimated $b_{bp}(\lambda)$: When $\Delta a(\lambda_0)$ is known, the uncertainty of $b_{bp}(\lambda_0)$, based on Eqs. (12a) and (6), is

$$b_{bp}(\lambda_0) = B(\lambda_0)\Delta a(\lambda_0), \tag{13a}$$

assuming B is error free. Equation (13a) indicates that the uncertainty of $b_{bp}(\lambda_0)$ is proportional to that of $a(\lambda_0)$.

The uncertainty of b_{bp} at other wavelengths, however, will be different because it depends on the accuracy of $\rho(\lambda, \lambda_0)$; see Eq. (7a). When $\rho(\lambda, \lambda_0)$ is described by Eq. (7b), the uncertainty of $b_{bp}(\lambda)$ then depends on the accuracy of η:

$$\Delta b_{bp}(\lambda) = \sqrt{\left(B(\lambda_0) \left(\frac{\lambda_0}{\lambda}\right)^{\eta} \Delta a(\lambda_0)\right)^2 + \left([B(\lambda_0)\, a(\lambda_0) - b_{bw}(\lambda_0)]\left(\frac{\lambda_0}{\lambda}\right)^{\eta} \ln\left(\frac{\lambda_0}{\lambda}\right)\Delta\eta\right)^2}. \tag{13b}$$

In Eq. (13b), the first term on the right-hand side is for $\Delta\eta = 0$, while the second term is for $\Delta a(\lambda_0) = 0$.

Note that Eq. (7b) is not error free in describing the spectral variation of $b_{bp}(\lambda)$, and this imperfection is lumped into the uncertainty of variable η. For two different wavelengths, e.g., 411 and 443 nm, it was found that $\rho(411, 555)$ is highly correlated with $\rho(443, 555)$ [$R^2 = 0.93$, NOMAD (the NASA bio-Optical Marine Algorithm Dataset [38]), not shown here]. It is thus justified to use the combination of Eq. (7b) and $\Delta\eta$ for the estimation of $\Delta\rho(\lambda, \lambda_0)$ and then $\Delta b_{bp}(\lambda)$.

b. Uncertainty in estimated $a(\lambda)$: The uncertainty of $a(\lambda)$ resulting from $\Delta a(\lambda_0)$ and $\Delta\eta$ is derived by combining Eqs. (9) and (13b), omitting uncertainties associated with quantities A and B, which are calculated from measured r_{rs} through Eqs. (1) and (2):

$$\Delta a(\lambda) = \sqrt{\left(A(\lambda)B(\lambda_0)\left(\frac{\lambda_0}{\lambda}\right)^{\eta}\Delta a(\lambda_0)\right)^2 + \left(A(\lambda)[B(\lambda_0)a(\lambda_0) - b_{bw}(\lambda_0)]\left(\frac{\lambda_0}{\lambda}\right)^{\eta}\ln\left(\frac{\lambda_0}{\lambda}\right)\Delta\eta\right)^2}. \tag{14}$$

Equations (13a), (13b), and (14) indicate that, in the QAA system, when both $a(\lambda_0)$ and η are error free [both $\Delta a(\lambda_0)$ and $\Delta\eta$ are zero], the derived backscattering coefficient and absorption at other wavelengths will also be error free. This suggests that, in addition to improving the qualities of r_{rs} measurements and r_{rs} models, we should focus on minimizing $\Delta a(\lambda_0)$ and $\Delta\eta$ in future efforts to improve QAA performance.

c. Uncertainties in estimated $a_{ph}(\lambda_2)$ and $a_{dg}(\lambda_2)$: Subsequently, we can analytically evaluate the propagated uncertainty in QAA-derived $a_{ph}(\lambda_2)$ and $a_{dg}(\lambda_2)$, respectively. Since $a_w(\lambda)$ are considered constants, there are four properties [see Eq. (10)] contributing to the uncertainties of QAA-derived $a_{ph}(\lambda_2)$ and $a_{dg}(\lambda_2)$: $a(\lambda_1)$, $a(\lambda_2)$, ζ, and ξ. The uncertainty contributions of ζ and ξ are treated independent of each other, as field observations have not demonstrated that ζ covaries with ξ in natural aquatic environments.

The uncertainty contributions of $a(\lambda_1)$ and $a(\lambda_2)$ to $\Delta a_{dg}(\lambda_2)$ and $\Delta a_{ph}(\lambda_2)$ are through the partial differences between $a(\lambda_1)$ and $a(\lambda_2)$ ($a(\lambda_1)$–$\zeta a(\lambda_2)$ and $\xi a(\lambda_2)$–$a(\lambda_1)$, respectively; see Eq. (10)). Therefore, it is necessary to know the algorithm-introduced uncertainty of the partial differences for analyzing $\Delta a_{dg}(\lambda_2)$ and $\Delta a_{ph}(\lambda_2)$. Define $a_{12\zeta}$ as

$$a_{12\zeta} = a(\lambda_1) - \zeta a(\lambda_2). \tag{15}$$

Then, after a simple mathematical manipulation, $a_{12\zeta}$ is

$$a_{12\zeta} = b_{bp}(\lambda_0)\left[A(\lambda_1)\left(\frac{\lambda_0}{\lambda_1}\right)^{\eta} - \zeta A(\lambda_2)\left(\frac{\lambda_0}{\lambda_2}\right)^{\eta}\right] + \sigma. \tag{16}$$

Here σ is

$$\sigma = A(\lambda_1)b_{bw}(\lambda_1) - \zeta A(\lambda_2)b_{bw}(\lambda_2), \quad (17)$$

which has no dependence on both $a(\lambda_0)$ and η.

Following Eq. (12b), when $b_{bp}(\lambda_0)$ and η have uncertainties, the uncertainty of $a_{12\zeta}$, $\Delta a_{12\zeta}$, is

$$\begin{aligned}(\Delta a_{12\zeta})^2 = &\left\{\Delta b_{bp}(\lambda_0)\left[A(\lambda_1)\left(\frac{\lambda_0}{\lambda_1}\right)^{\eta} - \zeta A(\lambda_2)\left(\frac{\lambda_0}{\lambda_2}\right)^{\eta}\right]\right\}^2 \\ &+ \left\{b_{bp}(\lambda_0)\left[A(\lambda_1)\left(\frac{\lambda_0}{\lambda_1}\right)^{\eta}\ln\left(\frac{\lambda_0}{\lambda_1}\right)\right.\right. \\ &\left.\left. - \zeta A(\lambda_2)\left(\frac{\lambda_0}{\lambda_2}\right)^{\eta}\ln\left(\frac{\lambda_0}{\lambda_2}\right)\right]\Delta\eta\right\}^2. \quad (18)\end{aligned}$$

Therefore, with $\Delta\zeta$ and $\Delta\xi$ for uncertainties of ζ and ξ, respectively, $\Delta a_{dg}(\lambda_2)$ is

$$\begin{aligned}(\Delta a_{dg}(\lambda_2))^2 = &\frac{(\Delta a_{12\zeta})^2}{(\xi-\zeta)^2} \\ &+ \left(\frac{a_{12\zeta} - a_w(\lambda_1) + \zeta a_w(\lambda_2)}{(\xi-\zeta)^2}\Delta\xi\right)^2 \\ &+ \left(\frac{a_w(\lambda_2) - a(\lambda_2)}{\xi-\zeta}\Delta\zeta\right. \\ &\left. + \frac{a_{12\zeta} - a_w(\lambda_1) + \zeta a_w(\lambda_2)}{(\xi-\zeta)^2}\Delta\zeta\right)^2. \quad (19)\end{aligned}$$

Similarly, for the uncertainty of $a_{ph}(\lambda_2)$, we define $a_{21\zeta}$ as $a_{21\xi} = \xi a(\lambda_2) - a(\lambda_1)$.

Thus, $\Delta a_{ph}(\lambda_2)$ is

$$\begin{aligned}(\Delta a_{ph}(\lambda_2))^2 = &\frac{(\Delta a_{21\xi})^2}{(\xi-\zeta)^2} \\ &+ \left(\frac{a_{21\xi} + a_w(\lambda_1) - \xi a_w(\lambda_2)}{(\xi-\zeta)^2}\Delta\zeta\right)^2 \\ &+ \left(\frac{a(\lambda_2) - a_w(\lambda_2)}{\xi-\zeta}\Delta\xi\right. \\ &\left. - \frac{a_{21\xi} + a_w(\lambda_1) - \xi a_w(\lambda_2)}{(\xi-\zeta)^2}\Delta\xi\right)^2, \quad (21)\end{aligned}$$

with

$$\begin{aligned}(\Delta a_{21\xi})^2 = &\left\{\Delta b_{bp}(\lambda_0)\left[\xi A(\lambda_2)\left(\frac{\lambda_0}{\lambda_2}\right)^{\eta} - A(\lambda_1)\left(\frac{\lambda_0}{\lambda_1}\right)^{\eta}\right]\right\}^2 \\ &+ \left\{b_{bp}(\lambda_0)\left[\xi A(\lambda_2)\left(\frac{\lambda_0}{\lambda_2}\right)^{\eta}\ln\left(\frac{\lambda_0}{\lambda_2}\right)\right.\right. \\ &\left.\left. - A(\lambda_1)\left(\frac{\lambda_0}{\lambda_1}\right)^{\eta}\ln\left(\frac{\lambda_0}{\lambda_1}\right)\right]\Delta\eta\right\}^2. \quad (22)\end{aligned}$$

In Eqs. (19) and (21), values of all parameters are given or derived from $r_{rs}(\lambda)$; consequently the uncertainties of QAA-derived $a_{dg}(\lambda_2)$ and $a_{ph}(\lambda_2)$ can be estimated for each $r_{rs}(\lambda)$. Because $a_{ph}(\lambda_2)$ and $a_{dg}(\lambda_2)$ are next level products from r_{rs} inversion [26], i.e., derivative products of $a(\lambda)$, uncertainties associated with inverted $a_{ph}(\lambda_2)$ and $a_{dg}(\lambda_2)$ are much more complex when compared to that of $b_{bp}(\lambda)$ or $a(\lambda)$.

3. Data to Quantify Uncertainties of Inherent Optical Properties Derived by Quasi-Analytical Algorithm

Ideally, error-free field measured data are used to derive and quantify uncertainties of algorithm-derived products. When an error-bearing data set is used, it is difficult to assign the difference between algorithm outputs and measurements to algorithm error or measurement error. Because there is no error-free data set from field measurements, and the purpose of this study is to isolate and evaluate uncertainties introduced by the algorithm alone, we simulated a data set that best represented natural variability, including both IOPs and r_{rs}, in a fashion similar to the International Ocean-Colour Coordinating Group (IOCCG) Algorithm Working Group [19].

Generation of the data set starts with the creation of spectral IOPs, b_b and a, in particular:

$$\begin{aligned}a(\lambda) &= a_w(\lambda) + a_{ph}(\lambda) + a_{dg}(\lambda), \\ b_b(\lambda) &= b_{bw}(\lambda) + b_{bp}(\lambda). \quad (23)\end{aligned}$$

Values for $a_w(\lambda)$ and $b_{bw}(\lambda)$ are already known [33,39], and the following optical models were used to create spectra of the other components:

$$\begin{aligned}a_{ph}(\lambda) &= a_{ph}(440)a^+_{ph}(\lambda), \\ a_{dg}(\lambda) &= a_{dg}(440)e^{-S(\lambda-440)}, \\ b_{\mathrm{bp}}(\lambda) &= b_{\mathrm{bp}}(440)\left(\frac{440}{\lambda}\right)^{\eta}. \quad (24)\end{aligned}$$

Here $a^+_{ph}(\lambda)$ is the $a_{ph}(440)$-normalized phytoplankton absorption coefficient, which provides a spectral shape for $a_{ph}(\lambda)$. Both $a_{ph}(440)$, in a range of ~0.0056–0.42 m^{-1}, and $a^+_{ph}(\lambda)$ were taken from the IOCCG database [19]. Although the spectral a_{dg} and b_{bp} models are idealistic, the small deviations are considered having negligible effects to the analyses here.

Because the estimation of $a(\lambda_0)$ in QAA depends completely on the spectral shape of $r_{rs}(\lambda)$, which is primarily determined by the shape and magnitudes of $a_{ph}(\lambda)$ and $a_{dg}(\lambda)$ (they are, in general, selectively stronger in the shorter wavelengths) and the shape of $b_{bp}(\lambda)$ (its magnitude is nearly canceled out in the r_{rs} band ratios), we systematically varied $a_{dg}(\lambda)$ and η for each $a_{ph}(\lambda)$, but left $b_{bp}(440)$ varying in a random way, similar to the IOCCG data set. Specifically, the magnitude parameters of $a_{dg}(440)$ and $b_{bp}(440)$ were determined as follows:

$$\begin{aligned}a_{dg}(440) &= p_1 a_{ph}(440), \\ b_{bp}(440) &= p_2(a_{ph}(440) + a_{dg}(440)). \quad (25)\end{aligned}$$

The value p_1, which describes the ratio of $a_{dg}(440)/a_{ph}(440)$, was varied from 0.2 to 7.0 with a step of 0.2 (35 p_1 values). The spectral slope of

$a_{dg}(\lambda)$, S, was varied from 0.01 to 0.02 with a step of 0.002 (6 S values). The spectral shape of $b_{bp}(\lambda)$, η, was varied from 0 to 2.0 with a step of 0.2 (11 η values). The value p_2 was used to generate $b_{bp}(440)$ (and then $b_{bp}(\lambda)$, when associated with values of η) and was determined by the following:

$$p_2 = 0.001 + \frac{0.3\Re a_{ph}(440)}{0.006 + a_{ph}(440)}, \tag{26}$$

with $\Re$ a random value between 0 and 1. Therefore p_2 is in a range between 0.001 and 0.3, and between 0.001 and 0.15 at the lower end and a wider range for larger $a_{ph}(440)$ values, in a way to mimic natural variations. In QAA, because $b_{bp}(\lambda)$ is analytically derived, the way of p_2 variation does not matter here, as long as the overall range is consistent with natural environments.

Based on the above setup, there are 2310 ($35 \times 6 \times 11$) combinations of $a_{dg}(\lambda)$ and $b_{bp}(\lambda)$ for each $a_{ph}(440)$ value. Since there are 20 different $a_{ph}(440)$ values in the IOCCG database, we created a data set with 46,200 combinations of $a_{ph}(\lambda)$, $a_{dg}(\lambda)$, and $b_{bp}(\lambda)$, and then $a(\lambda)$ and $b_b(\lambda)$. Note that $a_{ph}^{+}(\lambda)$ is not the same for the same $a_{ph}(440)$ value in the IOCCG database; thus the spectral variability of $a_{ph}(\lambda)$ within each group is maintained here.

After $a(\lambda)$ and $b_b(\lambda)$ are known, to be more efficient, $r_{rs}(\lambda)$ is modeled using Eq. (2) instead of using Hydrolight [40]. This is also because we are assuming a perfect analytical model between the apparent optical properties (AOP: $r_{rs}(\lambda)$) and the IOPs (b_b and a) and focusing on uncertainties of $a(\lambda_0)$ and η (and ζ and ξ) and their propagations in the QAA system. Indeed, there is a $<10\%$ error associated with Eq. (2) [29,41], which has a bigger effect on the retrieval of b_{bp} when b_{bp} is extremely small, e.g., for waters in the oceanic gyres [42]. However, errors associated with the r_{rs} model can be corrected later when a more accurate model is adopted (Lee *et al*, in preparation), and such a correction will not affect the general conclusions about the uncertainties of $a(\lambda_0)$, η, ζ, and ξ and their propagations to other IOPs.

The wavelengths used in this study (410, 440, 490, 550, and 670 nm) do not exactly match those from the current operational satellite sensors such as SeaWiFS/MODIS/MERIS. The spectral differences of the corresponding bands, however, are so small that results and conclusions achieved here are applicable to those ocean color systems. Figure 2(a) presents values and ranges of the simulated $a(440)$ and $a(550)$, and Fig. 2(b) illustrates values and ranges of $r_{rs}(440)$ and $r_{rs}(550)$. The figures also show equivalent data from field measurements (NOMAD) [38]. Both charts demonstrate a wide range of values at 440 nm for a given value at 550 nm, as expected in natural aquatic environments (simulated absorption actually has a wider range than current NOMAD values). These comparisons indicate that the simulated data set is consistent, in both magnitude and variability, with data from field measurements. A unique feature of the simulated data set, however, is that it is free of measurement errors, and thus well suited to identify and analyze algorithm introduced uncertainties.

4. Results and Discussion

A. Uncertainty in the Estimated $a(\lambda_0)$

As shown by Eq. (14), one key component in the QAA system is the estimation of $a(\lambda_0)$, because it is one of the properties that initiates the entire sequential process. Figure 3(a) illustrates derived $a(550)$ [from Eq. (5), 550 nm is considered λ_0 here; also note that sensor specific coefficients are required to obtain consistent results across different sensors] versus known $a(550)$. Because Eq. (5) is not perfect, there is an error (big or small) associated with each inverted $a(550)$. To highlight the range of errors between known and inverted $a(550)$, Fig. 3(b) shows the distribution of the absolute percentage error (ape): $|a(550)_{\text{known}} - a(550)_{\text{QAA}}|/a(550)_{\text{known}}$. About 57% of the data have an ape within ~13%, and about 70% of the data have an ape within 20%. The overall average of ape is 15.6%.

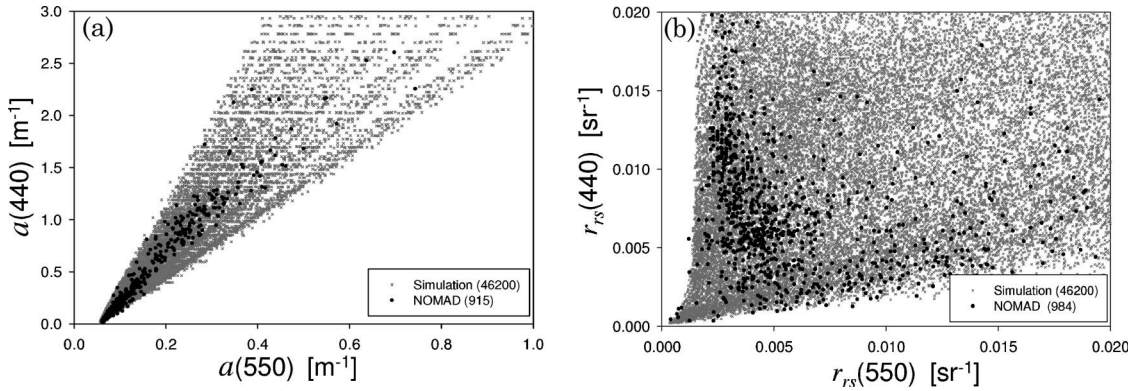

Fig. 2. Examples of simulated optical properties at 440 and 555 nm (a) for absorption coefficients and (b) for remote-sensing reflectance (subsurface). For comparison, corresponding values from the NOMAD data set [38] are also plotted. For NOMAD, there are 915 pairs of absorption coefficients, while there are 984 pairs of reflectance coefficients, but there are 46,200 pairs of values for the simulated data sets. The NOMAD r_{rs} values were converted from above-surface remote-sensing reflectance (R_{rs}) with $r_{rs} = R_{rs}/(0.52 + 1.7R_{rs})$.

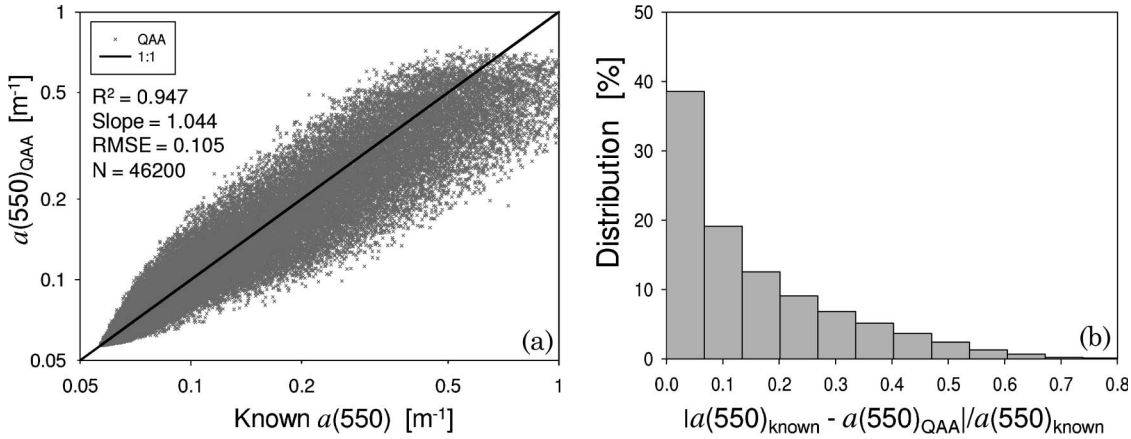

Fig. 3. (a) QAA-derived $a(550)$ compared with known $a(550)$ of the simulated data set. Statistics of data in log scale are shown in the figure. (b). Histogram of absolute percentage error in linear scale, $|a(550)_{\text{known}} - a(550)_{\text{QAA}}|/a(550)_{\text{known}}$. The average of this error is 15.6%.

To evaluate the error for different $a(550)$ values, we divided the data set into 30 groups that correspond to a narrow range of $a(550)$ (within $\pm 2\%$ of a designated $a(550)$). The designated $a(550)$ values are 0.058, 0.063, 0.069, …, 0.374, 0.389, to 0.405 m^{-1}, with an increase rate of ~8% at the lower end and ~4% at the higher end. As remotely the "true" $a(550)$ is unknown, the designation of $a(550)$ is based on QAA-derived values. Note that the $a(440)$ is in a range of ~0.013–0.085 m^{-1} for the group with $a(550) = 0.058\ \text{m}^{-1}$ (slightly higher than the absorption coefficient of pure water at this wavelength [33], 0.0565 m^{-1}), and is in a range of ~0.9–2.8 m^{-1} for the group with $a(550) = 0.405\ \text{m}^{-1}$. Such ranges indicate that the $a(550)$ range, ~0.058–0.4 m^{-1}, covers all oceanic and most coastal waters. We limited the analyses to $a(550)_{\text{QAA}} \leq \sim 0.4\ \text{m}^{-1}$ also because that QAA-derived $a(550)$ gradually plateaus at ~0.5 m^{-1}, which suggests that the current version of QAA contains higher uncertainties when QAA-derived $a(550) > 0.5\ \text{m}^{-1}$, i.e., for extremely turbid waters. For such cases, a reference wavelength longer than 550 nm is needed (e.g., Lee *et al.* [23] and Doron *et al.* [14]).

For each point, the absolute difference (ε), or error, between QAA-derived and known $a(550)$ is calculated:

$$\varepsilon = |a(550)_{\text{known}} - a(550)_{\text{QAA}}|, \tag{27}$$

along with its relative difference, i.e., $\varepsilon/a(550)_{\text{QAA}}$. As examples, Fig. 4 shows the distributions of $\varepsilon/a(550)_{\text{QAA}}$ for six groups with different $a(550)_{\text{QAA}}$ values. For this simulated data set with the current version of QAA, the relative differences, $\varepsilon/a(550)_{\text{QAA}}$, are centered at the lower end of the values. In particular, for waters with low $a(550)_{\text{QAA}} (< 0.076\ \text{m}^{-1})$, 70% or more of the true $a(550)$ are within $\pm 10\%$ of $a(550)_{\text{QAA}}$; when $a(550)_{\text{QAA}}$ becomes larger, e.g., 0.2 m^{-1} or more, some of the true $a(550)$ could be off by $\pm 60\%$ of $a(550)_{\text{QAA}}$. These results demonstrate that the errors or uncertainties in ocean color remote sensing are not uniform, as recently found by Moore *et al.* [9] when empirically retrieved chlorophyll-a concentrations were evaluated.

The uncertainty of QAA-derived $a(550)$, $\Delta a(550)$, is defined as the average of ε for each group because it approximates the 65th percentile of the ε distribution; see Fig. 5. By this definition, there is a 65% likelihood that the "true" $a(550)$ will be within $a(550)_{\text{QAA}} \pm \Delta a(550)$. Figure 5 shows the relative uncertainties $(\Delta a(550))/a(550)_{\text{QAA}}$, with $a(550)_{\text{QAA}}$ the average $a(550)_{\text{QAA}}$ of each group) for the various $a(550)$ groups. For $a(550)_{\text{QAA}} < 0.1\ \text{m}^{-1}$, which covers ~95% of global waters (Bryan Franz, personal communication), $\Delta a(550)/a(550)_{\text{QAA}}$ is in general <16%. Since $a(550)$ is dominated by the contribution of pure water, the uncertainty associated with QAA derived $a(550)$ is limited for most oceanic waters. On the

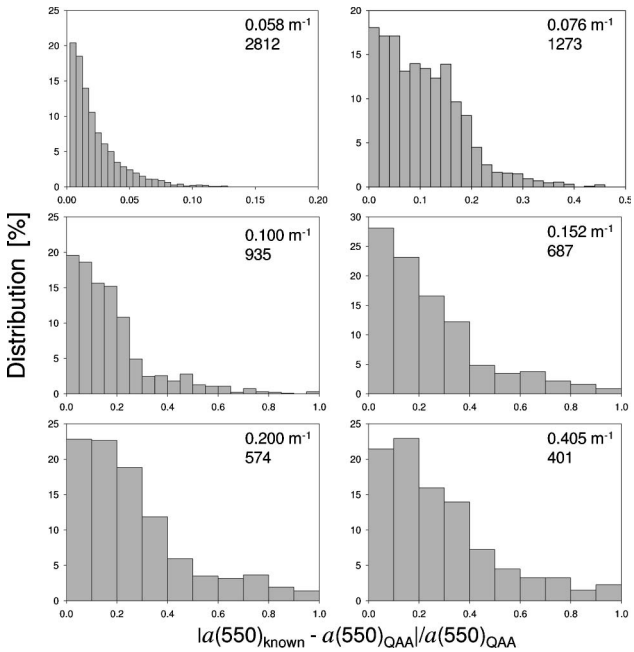

Fig. 4. Histograms of $|a(550)_{\text{known}} - a(550)_{\text{QAA}}|/a(550)_{\text{QAA}}$ for a few designated $a(550)_{\text{QAA}}$ values. The first value in a figure represents $a(550)_{\text{QAA}}$, and the second value represents the number of points for that $a(550)_{\text{QAA}}$ group (see text for details).

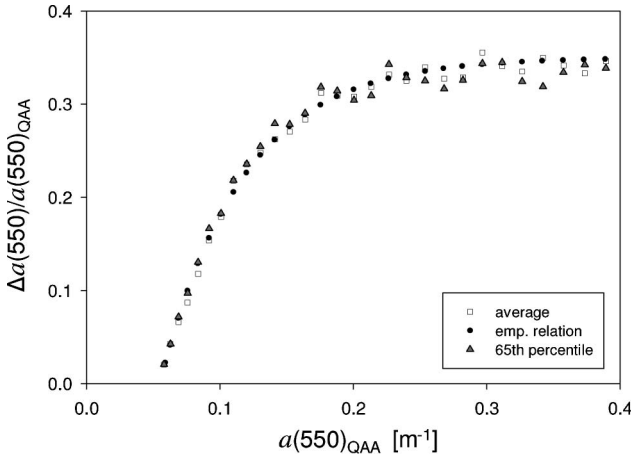

Fig. 5. Relationships between $\Delta a(550)/a(550)_{QAA}$ and $a(550)_{QAA}$ for $a(550)_{QAA}$ up to $0.4\,m^{-1}$. The values of $\Delta a(550)$ from two different calculations are presented; one (open square) is the average of $|a(550)_{known} - a(550)_{QAA}|$ of each group, and the other (gray triangle) is the 65th percentile of $|a(550)_{known} - a(550)_{QAA}|$ of each group. The solid dots represent an empirical fit [Eq. (28) divided by $a(550)_{QAA}$] for easy evaluation of $\Delta a(550)$.

other hand, uncertainties are higher [larger $\Delta a(550)$] for higher $a(550)$ values, where marine optical and biogeochemical properties are more complex.

To derive $\Delta a(550)$ for any given $a(550)_{QAA}$, a best-fit empirical relationship between $\Delta a(550)$ and $a(550)_{QAA}$ was derived (dotted line in Fig. 5):

$$\Delta a(550) \approx 0.35(1 - 2.4\exp(-16.0\,a(550)_{QAA})) \times a(550)_{QAA}. \quad (28)$$

Because $a(550)$ in our simulated data set has a wider range and higher variability than in the NOMAD data set (see Fig. 2), $\Delta a(550)$ of real environments could be smaller than that represented by Eq. (28), assuming high-quality r_{rs}.

In the above analysis the number of points of each group spans from 2812 [$a(550)_{QAA} = 0.058\,m^{-1}$] to 401 [$a(550)_{QAA} = 0.405\,m^{-1}$]. To test the effect of the number of points on the evaluation of $\Delta a(550)$, we changed the lower-upper bounds of each group from within $\pm 2\%$ to within $\pm 5\%$ of the designated $a(550)$, resulting in nearly double the number of points for each group [4873 for $a(550)_{QAA} = 0.058\,m^{-1}$, and 962 for $a(550)_{QAA} = 0.405\,m^{-1}$]. We found negligible effects to the statistical results shown in Fig. 5, which provides confidence that $\Delta a(550)$ values shown in Fig. 5 are not sensitive to $a(550)$ grouping so long as narrow bounds are maintained.

B. Uncertainty in the Estimated $b_{bp}(\lambda_0)$

With $\Delta a(550)$ known, the uncertainty of $b_{bp}(550)$ can be easily calculated [see Eq. (13a)]. Figure 6(a) presents the relative uncertainties of $b_{bp}(550)$ [$\Delta b_{bp}(550)/b_{bp}(550)_{QAA}$] of the simulated data set, which are generally in a range of ~2–40%, but can approach infinity when derived $b_{bp}(550)$ nears zero. Although $\Delta a(550)$ is fixed for a given $a(550)_{QAA}$, the relative uncertainty of $b_{bp}(550)$ differs for the same QAA-derived $b_{bp}(550)$ values. This can be explained, combining Eqs. (6) and (13a), by

$$\frac{\Delta b_{bp}(550)}{b_{bp}(550)_{QAA}} = \frac{B(550)\Delta a(550)}{B(550)a(550)_{QAA} - b_{bw}(550)}. \quad (29)$$

Different combinations of $B(550)$ and $a(550)_{QAA}$ can result in the same $b_{bp}(550)$. Different $a(550)_{QAA}$ values, however, come with different $\Delta a(550)$ values, and $B(550)$ does not cancel out in Eq. (29) until $b_{bw}(550)$ is negligible, which therefore results in different $\Delta b_{bp}(550)$.

To illustrate how QAA performs for oceanic waters, Figure 6(b) shows the relative uncertainties of $b_{bp}(550)$ for data with $a(550) \le 0.065\,m^{-1}$ and indicates that generally the relative uncertainty is less than or around $\pm 10\%$ for $b_{bp}(550)_{QAA}$ in the range of 0.0003–0.003 m^{-1}. Such a result suggests that theoretically highly reliable $b_{bp}(550)$ can be retrieved from spectral remote sensing reflectance for such waters by QAA. For realistic systems, however, the accuracy of $b_{bp}(550)$ also depends on the accuracy of $B(550)$ and the absorption [33,43] and backscattering coefficients [44,45] of pure water.

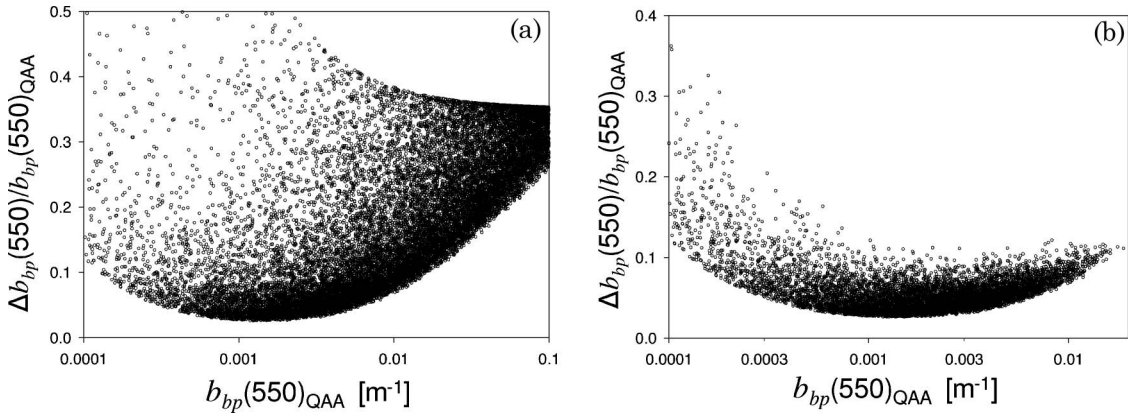

Fig. 6. Relative uncertainty of QAA-derived $b_{bp}(550)$ (a) for the entire simulated data set and (b) for data with $a(550) < 0.065\,m^{-1}$.

C. Uncertainty in the Estimated $a(\lambda)$

The calculation of $\Delta a(\lambda)$ requires knowledge of the uncertainty of $\Delta\rho(\lambda,\lambda_0)$, which is represented by $\Delta\eta$ [Eq. (14)]. Unfortunately, the spatial variability of $\Delta\eta$ is unknown, although global maps of η have been produced [23,46]. Also, there is not enough high-quality measured data to evaluate a confidence range of η for various regions, although the expression [Eq. (8)] generally captures the trend of higher values in oceanic waters and lower values in coastal waters [47]. Unlike the total absorption coefficients that have a general spectral dependence, governed by the spectral shapes of the multiple components, η is a parameter used to determine the spectral dependence of b_{bp}. Therefore, unlike $\Delta a(\lambda_0)$, $\Delta\eta$ could not be evaluated with a simulated data set. Instead, based on a comparison (not presented here) between r_{rs} estimated η [Eq. (8)] and calculated η from measured $b_{bp}(\lambda)$ of the NOMAD data set, a $\Delta\eta = 0.5$, which represents the 68th percentile of the absolute η difference, was assigned universally. This assigned value represents a high variability; i.e., if the true η value is 1.0, $\Delta\eta = 0.5$ suggests an η range of 0.5–1.5 [$\rho(440,550)$, range of ~1.12–1.40] for 68% of the samples, which cover nearly all waters.

To show the different contributions of $\Delta a(\lambda_0)$ and $\Delta\eta$ to $\Delta a(\lambda)$, Eq. (14) is applied to the simulated data set. As an example, $\Delta a(440)$ is calculated with $\Delta a(550)$ and $\Delta\eta$ separately, and then calculated with both. Figure 7 presents their relative contributions and the combined effects, with the Y axis for $\Delta a(440)/a(440)_{QAA}$, the relative uncertainty. Clearly, 1) there are different $\Delta a(440)$ for the same $a(440)_{QAA}$ (see Fig. 7), as its inversion is also associated with particle scattering properties, and 2) $\Delta a(550)$ and $\Delta\eta$ contribute differently to $\Delta a(440)$. For relatively clear waters [$a(550) < 0.08\,m^{-1}$], because $a(550)_{QAA}$ is quite accurate, the contribution of $\Delta a(550)$ to $\Delta a(440)$ is limited (the blue dots in Fig. 7). The contribution of $\Delta\eta$ to $\Delta a(440)$, on the other hand, could be higher than that from $\Delta a(550)$, as its effect also depends on the value of $B(550)$, which is directly related to the value of $r_{rs}(550)$ and the r_{rs} model used. For coastal turbid waters, however, the maximum contribution from $\Delta\eta$ is ~11%, which approximates the square root of 550/440. But $\Delta a(550)$ in general contributes more to $\Delta a(440)$ for complex waters, simply because $\Delta a(550)$ itself gets larger. Note that for a specific case, because the overestimation or underestimation of $a(\lambda_0)$ or η are not necessarily in phase for a measured $r_{rs}(\lambda)$, the effects of errors in $a(\lambda_0)$ and η on $b_{bp}(\lambda)$ and $a(\lambda)$ are not necessarily compounded. If one is overestimated while the other is underestimated, the actual error in the derived $b_{bp}(\lambda)$ and $a(\lambda)$ could be minimal.

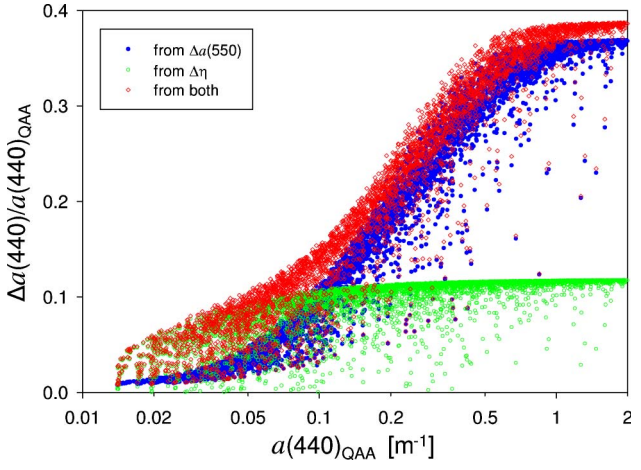

Fig. 7. (Color online) Relationship between relative uncertainty of $a(440)$[$\Delta a(440)/a(440)_{QAA}$, red] and QAA-derived $a(440)$. Also shown are contributions of $\Delta a(550)$ (blue) and $\Delta\eta$ (green), respectively, to the relative uncertainty.

The above results suggest that for waters with $a(440)_{QAA} \le 0.05\,m^{-1}$ (most oceanic waters, Bryan Franz, personal communication), the "true" $a(440)$ value is most likely within ±9% of $a(440)_{QAA}$, and could be within ±2% of $a(440)_{QAA}$, if r_{rs} measurements and models are highly reliable. This result and the result about $b_{bp}(550)$ indicate that since r_{rs} is a cumulative measure of the upper tens of meters of such waters [48], r_{rs} inversion is an efficient and reliable sampling method for measurement of optical properties of many oceanic waters. Note that traditional water sampling approaches require either long path-length tubes (e.g., ac-9, Wetlabs, Inc.) or a large volume of water samples [49,50] to obtain reliable *in situ* measurements for such waters.

Separately, because the diffuse attenuation coefficient of downwelling irradiance (K_d) is a simple function of a and b_b [51,52], the above analysis can easily be extended to evaluate the uncertainties associated with the semianalytically derived K_d products [51,52].

D. Uncertainty in the Estimated $a_{dg}(440)$ and $a_{ph}(440)$

The uncertainties of $a_{dg}(440)$ and $a_{ph}(440)$ are associated with both the uncertainties of the QAA-derived $a(\lambda)$ and the uncertainties of parameters ζ and ξ. The parameter ζ varies in a relatively small range (0.7–1.0) based on field measurements [53], but ξ could have much wider variations. When fitting measured $a_{dg}(\lambda)$ with an exponential function, the spectral slope (S) is generally in a range of 0.01–0.02 nm^{-1} [49,54–56], which suggests a range of ~1.35–1.82 for ξ. Because it is not clear yet how to best assign values for both ζ and ξ for an individual pixel, we chose to assign a constant value of 0.85 for ζ (the mode of NOMAD, not shown here) and 1.568 for ξ, which is equivalent to $S = 0.015\,nm^{-1}$, or a power value of 6.8 when $a_{dg}(\lambda)$ is fitted with a power-law function of wavelength [56]. Further, we set a universal uncertainty of $\Delta\zeta$ as 0.1 and $\Delta\xi$ as 0.14, which indicates a ζ range of 0.75–0.95 and a ξ range of 1.43–1.71 (equivalent S range of 0.012–0.018 nm^{-1}); both cover a majority of ocean waters. Note that these values and ranges could be refined later after we acquire additional knowledge about their ways of variations.

With the above values for ζ, ξ, $\Delta\zeta$, $\Delta\xi$, and $\Delta a(550)$ and $\Delta\eta$ for each $r_{rs}(\lambda)$, values of $\Delta a_{dg}(440)$ and Δa_{ph}

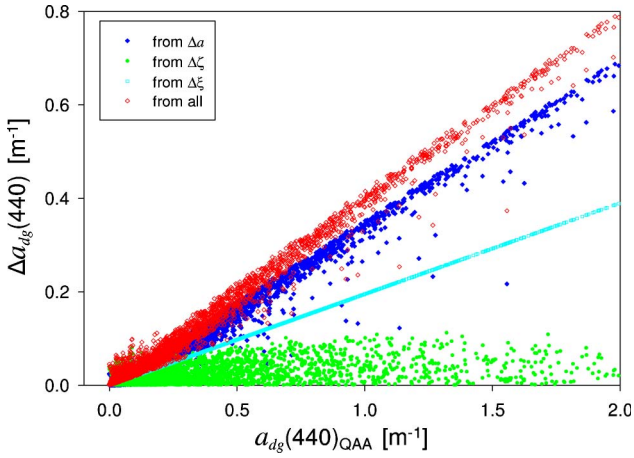

Fig. 8. (Color online) Uncertainty of QAA-derived $a_{dg}(440)$. Also shown are the contributions of Δa, $\Delta\zeta$, and $\Delta\xi$, respectively.

(440) were calculated and are presented in Figs. 8 and 9(a). The separate contributions of $\Delta\zeta$, $\Delta\xi$, and Δa are also presented in order to demonstrate their relative importance in $\Delta a_{dg}(440)$ and $\Delta a_{ph}(440)$, respectively. We do not present percentage-like error for $a_{dg}(440)$, or $a_{ph}(440)$, as shown in Figs. 5–7, because when $a(410)$ and $a(440)$ encounter larger errors, it can numerically result in negative or close to zero values (~8% of this data set), or very large values, for $a_{dg}(440)$ [or $a_{ph}(440)$] (commonly referred to as nonvalid retrieval in semianalytical algorithms [20,22,27]). Dividing $\Delta a_{dg}(440)$ [or $\Delta a_{ph}(440)$] to such QAA-derived $a_{dg}(440)$ [or $a_{ph}(440)$] values could result in a misleading perspective of relative uncertainty. The $\Delta a_{dg}(440)$ [or $\Delta a_{ph}(440)$] values, along with their corresponding $a_{dg}(440)$ [or $a_{ph}(440)$] values, provide adequate information about the reliability of $a_{dg}(440)$ [or $a_{ph}(440)$] derived from a spectral r_{rs}.

A few important findings can be drawn from the results shown Figs. 8 and 9(a):

a. Not surprisingly, $\Delta a_{dg}(440)$ and $\Delta a_{ph}(440)$ vary a lot. Their values and distributions are different from each other, and different for the same QAA-derived $a_{dg}(440)$ and $a_{ph}(440)$ values, respectively, i.e., nonuniform uncertainties. And, for the same QAA-derived $a_{dg}(440)$ and $a_{ph}(440)$ values, $\Delta a_{dg}(440)$ is apparently smaller than $\Delta a_{ph}(440)$. For instance, when QAA-$a_{dg}(440)$ is $0.1\,m^{-1}$, $\Delta a_{dg}(440)$ could be as low as $0.02\,m^{-1}$, or as high as $0.09\,m^{-1}$. When QAA-$a_{ph}(440)$ is $0.1\,m^{-1}$, however, $\Delta a_{ph}(440)$ could be in a range of 0.02–0.7 m^{-1}. Such a result suggests that fundamentally we could do better in analytically retrieving a_{dg} than retrieving a_{ph}. The results also highlight the importance and necessity of obtaining quality measurements for each inverted a_{dg} and a_{ph} from $r_{rs}(\lambda)$.

b. Between $\Delta a_{dg}(440)$ and $\Delta a_{ph}(440)$, it is interesting that $\Delta a_{dg}(440)$ generally increases with QAA-derived $a_{dg}(440)$, but not QAA-derived $\Delta a_{ph}(440)$. This is primarily because the inversion of $a_{dg}(440)$ is proportional to $a(\lambda_1)$–$\zeta a(\lambda_2)$, while inversion of $a_{ph}(440)$ is proportional to $\xi a(\lambda_2)$–$a(\lambda_1)$ [see Eq. (10)]. When absorption in the blue domain is actually composed with high a_{dg} that is also associated with a large ξ value, say ~1.8 (equivalent S value of $0.019\,nm^{-1}$) and then $a(\lambda_1) \sim 1.8a(\lambda_2)$, it may result in very small or negative $a_{ph}(440)$ when a ξ value of 1.568 (equivalent S of $0.015\,nm^{-1}$) is used in QAA (or other model-based analytical inversion methods). For such a case, although the QAA-derived $a_{ph}(440)$ could be near zero or negative, $\Delta a_{ph}(440)$ could be very large, from a large Δa.

c. Obviously $\Delta\zeta$, $\Delta\xi$, and Δa all contribute to $\Delta a_{dg}(440)$ and $\Delta a_{ph}(440)$. It is worth noting, however, that $\Delta\xi$ and Δa generally contribute more than $\Delta\zeta$. In most cases, Δa values contribute more than $\Delta\xi$. This is because, since ξ is much larger than ζ, a small change in $a(\lambda)$ could more strongly affect $a_{ph}(440)$. Sometimes $\Delta\xi$ could contribute more than Δa to $\Delta a_{ph}(440)$, again when a_{dg} dominates. These results suggest that, as a first order estimation, it is justified to use universal default ζ and ξ values for operational processing ocean color images of global oceans. For further improvement in analytically deriving a_{ph} from r_{rs}, it is more important to get a better estimation of ξ (or S) rather than ζ.

d. Figure 9(a) also highlights the potentially high uncertainties associated with $a_{ph}(440)$ when it is algebraically derived from the blue portion of an

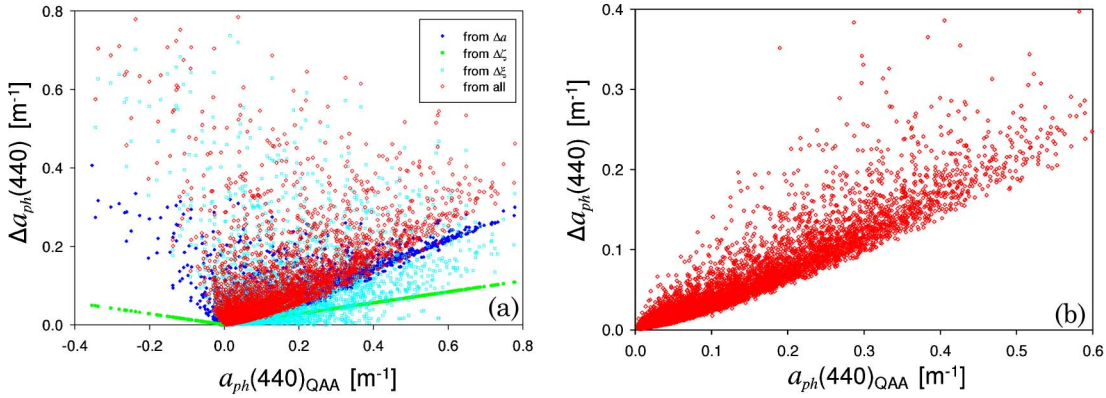

Fig. 9. (Color online) Uncertainty of QAA-derived $a_{ph}(440)$ (a) for the entire simulated data set, with contributions of Δa, $\Delta\zeta$, and $\Delta\xi$, respectively; (b) for data with $0.06 \le a_{dg}(440)/a_{ph}(440) \le 2$ and $1.43 \le a_{dg}(410)/a_{dg}(440) \le 1.72$.

r_{rs} spectrum, especially when water's absorption coefficient is dominated by the contribution from gelbstoff and/or detritus. In order to mitigate the uncertainties associated with analytical a_{ph} inversion for such environments, other approaches may be necessary. These include utilization of fluorescence line height [12,57], or using r_{rs} information at other bands, by incorporating spectral $a_{ph}(\lambda)$ models [22,30,53] to add spectral constraints. Each spectral model will introduce its own uncertainties because it is still not certain about which spectral model for $a_{ph}(\lambda)$ should be used for a specific water body.

e. On the other hand, if we restrict the analysis to data with $0.6 \le a_{dg}(440)/a_{ph}(440) \le 2.0$ and $1.43 \le \xi \le 1.72$ (equivalent to $0.012 \le S \le 0.018\,\mathrm{nm}^{-1}$) i.e., waters usually encountered in the open ocean [58], the uncertainties of $a_{ph}(440)$ are much narrower [see Fig. 9(b)]. Such results support the strategy of using $r_{rs}(\lambda)$ in the blue domain to analytically derive $a_{ph}(440)$ for most oceanic waters.

5. Summary and Conclusions

Based on the algebraic and stepwise nature of QAA and theory of error propagation, we developed analytical expressions [Eqs. (13a), (13b), (14), (19), (21), and (28)] for uncertainties of QAA-derived IOPs. These expressions provide the basis to evaluate and understand the uncertainties associated with analytically derived IOPs from remote sensing reflectance. Applying the expressions to a simulated wide-range data set, we evaluated and illustrated the uncertainties and their propagations associated with the QAA procedure and products. Specifically, we evaluated the uncertainties involved with the QAA-derived $a(\lambda_0)$, and further the propagation of $\Delta a(\lambda_0)$ and $\Delta\eta$ (when $b_{bp}(\lambda)$ is expressed as a power-law function) to other analytically derived IOPs. We found that the effects of these two on $a(\lambda)$ are different with $\Delta\eta$, potentially having a larger effect than $\Delta a(\lambda_0)$ for waters with a low absorption coefficient but high scattering coefficients, while $\Delta a(\lambda_0)$ has a larger effect for coastal waters. In general, with the current version of QAA and assuming that r_{rs} measurements and models are error free, the most likely uncertainty of QAA-derived $a(440)$ is under $\pm 13\%$ for $a(440)_{QAA} < 0.1\,\mathrm{m}^{-1}$ but can be as much as $\pm 37\%$ for $a(440)_{QAA}$ approaching $0.5\,\mathrm{m}^{-1}$. However, such uncertainties are not necessarily the same for waters with the same $a(\lambda)_{QAA}$ values, since the uncertainty of QAA-derived $a(\lambda)$ also depends upon the value of b_{bp}, and higher b_{bp} could cause larger uncertainty (resulting from error in b_{bp} extrapolation). For oceanic waters where particle backscattering is low, such as oceanic gyres [42], an uncertainty of ± 5–10% in QAA-derived $a(440)$ is expected.

Uncertainties of a_{dg} and a_{ph} are much more complex from ocean color inversion, as their accuracies depend not only on the accuracy of $a(\lambda)$ and their relative contributions to $a(\lambda)$, but also on their spectral dependencies. There could be significantly high uncertainties associated with algebraically derived a_{dg} or a_{ph}, if the total absorption has a high uncertainty and/or one of the two components dominates the other. However, if $a_{dg}(440)$ and $a_{ph}(440)$ are comparable to each other, e.g., the ratio of one to the other is between 0.5 and 2, it is well justified that both properties could be well retrieved, analytically, from the blue portion of $r_{rs}(\lambda)$. But, generally, for the same $a_{dg}(440)$ and $a_{ph}(440)$ values, it is found that uncertainties associated with $a_{dg}(440)$ are smaller than that of $a_{ph}(440)$.

For accurate derivation of a_{dg} and a_{ph}, the key components are the accurate total absorption coefficients in the blue/green domain and the spectral ratio of a_{dg} of the relevant wavelengths. For the derivation of a_{ph} in complex waters where a_{ph} is not the primary contributor to the total absorption, methods/approaches other than simple algebraic inversions are required to improve the quality of a_{ph} retrieval.

These quality measures can be extended to biogeochemical products, such as chlorophyll concentration), when the uncertainties between the optical properties and biogeochemical products are known per pixel. Although the evaluation results, especially for $\Delta a(550)$, might be dependent on the spectral models as well as the ranges and distributions of data used, the ranges of the parameters, S and η in particular, of the simulated data set are quite inclusive based on our current understanding, and therefore the results and conclusions are general and applicable to global oceans. Modifications and refinements are possible and expected when better parameterizations regarding $a(\lambda_0)$, $\rho(\lambda, \lambda_0)$, and ζ and ξ for various regions are developed.

This study shows that we can not only derive IOPs from the various ocean color missions, but also have necessary components for quantitatively measuring the quality of such IOP products for each pixel. The eventual generation of IOP quality maps, however, will depend on our understanding and quantification of the uncertainties of r_{rs} derived from various platforms over various waters [7,36,37], as well as uncertainties associated with r_{rs} models [41,59,60]. When the uncertainties of these variables are available pixelwise, they can be incorporated following the theory of error propagation for the generation of IOP quality maps from satellite ocean color remote sensing.

The authors are grateful for the financial support provided by NASA's Biology and Biogeochemistry and Water- and Energy Cycle Programs and by the Naval Research Laboratory. We also thank Emmanuel Boss and an anonymous reviewer for the comments and suggestions that greatly improved the manuscript.

References

1. International Ocean-Colour Coordinating Group, "Why ocean colour? The societal benefits of ocean-colour technology," in *Reports of the International Ocean-Colour Coordinating Group, No. 7*, T. Platt, N. Hoepffner, V. Stuart, and C. Brown, eds. (IOCCG, 2008).

2. International Ocean-Colour Coordinating Group, "Minimum requirements for an operational ocean-color sensor for the open ocean," in *Reports of the International Ocean-Color Coordinating Group, No. 1*, A. Morel, ed. (IOCCG, 1998).
3. International Ocean-Colour Coordinating Group, "Remote sensing of ocean colour in coastal, and other optically-complex, waters," in *Reports of the International Ocean-Colour Coordinating Group, No.3*, S. Sathyendranath, ed. (IOCCG, 2000).
4. E. S. Boss and S. Maritorena, "Uncertainties in the products of ocean-colour remote sensing," in *Remote Sensing of Inherent Optical Properties: Fundamentals, Tests of Algorithms and Applications*, Z.-P. Lee, ed. (IOCCG, 2006).
5. M. Chami and M. Defoin-Platel, "How ambiguous is the inverse problem of ocean color in coastal waters?," J. Geophys. Res. **112**, C03004 (2007).
6. M. S. Salama and A. Stein, "Error decomposition and estimation of inherent optical properties," Appl. Opt. **48**, 4947–4962 (2009).
7. D. Antoine, F. d'Ortenzio, S. B. Hooker, G. Becu, B. Gentili, D. Tailliez, and A. J. Scott, "Assessment of uncertainty in the ocean reflectance determined by three satellite ocean color sensors (MERIS, SeaWiFS and MODIS-A) at an offshore site in the Mediterranean Sea (BOUSSOLE project)," J. Geophys. Res. **113**, C07013 (2008).
8. J. O'Reilly, S. Maritorena, B. G. Mitchell, D. Siegel, K. L. Carder, S. Garver, M. Kahru, and C. McClain, "Ocean color chlorophyll algorithms for SeaWiFS," J. Geophys. Res. **103**, 24937–24953 (1998).
9. T. S. Moore, J. W. Campbell, and M. D. Dowell, "A class-based approach to characterizing and mapping the uncertainty of the MODIS ocean chlorophyll product," Remote Sens. Environ. **113**, 2424–2430 (2009).
10. T. Platt and S. Sathyendranath, "Oceanic primary production: estimation by remote sensing at local and regional scales," Science **241**, 1613–1620 (1988).
11. M. J. Behrenfeld, E. Boss, D. Siegel, and D. M. Shea, "Carbon-based ocean productivity and phytoplankton physiology from space," Global Biogeochem, Cycles **19**, GB1006 (2005).
12. C. Hu, F. E. Muller-Kager, G. A. Vargo, M. B. Neely, and E. Johns, "Linkages between coastal runoff and the Florida Keys ecosystem: a study of a dark plume event," Geophys. Res. Lett. **31**, L15307 (2004).
13. Z. P. Lee, A. Weidemann, J. Kindle, R. Arnone, K. L. Carder, and C. Davis, "Euphotic zone depth: its derivation and implication to ocean-color remote sensing," J. Geophys. Res. **112**, C03009 (2007).
14. M. Doron, M. Babin, A. Mangin, and O. Hembise, "Estimation of light penetration, and horizontal and vertical visibility in oceanic and coastal waters from surface reflectance," J. Geophys. Res. **112**, C06003 (2007).
15. G. Chang and A. L. Whitmire, "Effects of bulk particle characteristics on backscattering and optical closure," Opt. Express **17**, 2132–2142 (2009).
16. W. W. Gregg and M. E. Conkright, "Decadal changes in global ocean chlorophyll," Geophys. Res. Lett. **29**, 1730 (2002).
17. C. R. McClain, R. A. Barnes, J. R. E. Eplee, B. A. Franz, N. C. Hsu, F. S. Patt, C. M. Pietras, W. D. Robinson, B. D. Schieber, G. M. Schmidt, M. Wang, S. W. Bailey, and P. J. Werdell, "SeaWiFS postlaunch calibration and validation analyses, Part 2," NASA Tech. Memo. 2000-206892, S. B. Hooker, and E. R. Firestone, eds. (NASA Goddard Space Flight Center, 2000), Vol. 10, p. 57.
18. H. R. Gordon and M. Wang, "Retrieval of water-leaving radiance and aerosol optical thickness over oceans with SeaWiFS: A preliminary algorithm," Appl. Opt. **33**, 443–452 (1994).
19. International Ocean-Colour Coordinating Group, "Remote sensing of inherent optical properties: fundamentals, tests of algorithms, and applications," in *Reports of the International Ocean-Colour Coordinating Group, No. 5*, Z.-P. Lee, ed. (IOCCG, 2006), p. 126.
20. P. Wang, E. Boss, and C. Roesler, "Uncertainties of inherent optical properties obtained from semi-analytical inversions of ocean color," Appl. Opt. **44**, 4074–4085 (2005).
21. H. R. Gordon, "Normalized water-leaving radiance: revisiting the influence of surface roughness," Appl. Opt. **44**, 241–248 (2005).
22. F. E. Hoge and P. E. Lyon, "Satellite retrieval of inherent optical properties by linear matrix inversion of oceanic radiance models: an analysis of model and radiance measurement errors," J. Geophys. Res. **101**, 16631–16648 (1996).
23. Z. P. Lee, K. L. Carder, and R. Arnone, "Deriving inherent optical properties from water color: a multiband quasi-analytical algorithm for optically deep waters," Appl. Opt. **41**, 5755–5772 (2002).
24. S. L. Meyer, "*Data Analysis for Scientists and Engineers* (Wiley, 1975).
25. H. R. Gordon and A. Morel, *Remote Assessment of Ocean Color for Interpretation of Satellite Visible Imagery: A Review* (Springer-Verlag, 1983), p. 44.
26. R. Zaneveld, A. Barnard, and Z.-P. Lee, "Why are inherent optical properties needed in ocean-colour remote sensing," in *Remote Sensing of Inherent Optical Properties: Fundamentals, Tests of Algorithms and Applications*, Z.-P. Lee, ed. (IOCCG, 2006).
27. S. Maritorena, D. A. Siegel, and A. R. Peterson, "Optimization of a semianalytical ocean color model for global-scale applications," Appl. Opt. **41**, 2705–2714 (2002).
28. K. L. Carder, F. R. Chen, Z. P. Lee, S. K. Hawes, and D. Kamykowski, "Semianalytic Moderate-Resolution Imaging Spectrometer algorithms for chlorophyll-a and absorption with bio-optical domains based on nitrate-depletion temperatures," J. Geophys. Res. **104**, 5403–5421 (1999).
29. H. R. Gordon, O. B. Brown, R. H. Evans, J. W. Brown, R. C. Smith, K. S. Baker, and D. K. Clark, "A semianalytic radiance model of ocean color," J. Geophys. Res. **93**, 10909–10924 (1988).
30. Z. P. Lee, K. L. Carder, C. D. Mobley, R. G. Steward, and J. S. Patch, "Hyperspectral remote sensing for shallow waters. 1. A semianalytical model," Appl. Opt. **37**, 6329–6338 (1998).
31. A. Morel and B. Gentili, "Diffuse reflectance of oceanic waters (2): Bi-directional aspects," Appl. Opt. **32**, 6864–6879 (1993).
32. J. R. V. Zaneveld, "A theoretical derivation of the dependence of the remotely sensed reflectance of the ocean on the inherent optical properties," J. Geophys. Res. **100**, 13135–13142 (1995).
33. R. Pope and E. Fry, "Absorption spectrum (380–700 nm) of pure waters: II. Integrating cavity measurements," Appl. Opt. **36**, 8710–8723 (1997).
34. R. C. Smith and K. S. Baker, "Optical properties of the clearest natural waters," Appl. Opt. **20**, 177–184 (1981).
35. H. R. Gordon, "Radiometric considerations for ocean color remote sensors," Appl. Opt. **29**, 3228–3236 (1990).
36. C. Hu, K. L. Carder, and F. E. Muller-Karger, "How precise are SeaWiFS ocean color estimates? Implications of digitization-noise errors," Remote Sens. Environ. **76**, 239–249 (2001).
37. G. Zibordi, S. B. Hooker, J. F. Berthon, and D. D'Alimonte, "Autonomous above-water radiance measurements from an offshore platform: a field assessment experiment," J. Atmos. Oceanic Technol. **19**, 808–819 (2002).
38. P. J. Werdell and S. W. Bailey, "An improved bio-optical data set for ocean color algorithm development and satellite data product validation," Remote Sens. Environ. **98**, 122–140 (2005).
39. A. Morel, "Optical properties of pure water and pure sea water," in *Optical Aspects of Oceanography*, N. G. Jerlov and E. S. Nielsen, eds. (Academic, 1974), pp. 1–24.

40. C. D. Mobley, *Hydrolight 3.0 Users' Guide* (SRI International, 1995).
41. Z. P. Lee, K. L. Carder, and K. P. Du, "Effects of molecular and particle scatterings on model parameters for remote-sensing reflectance," Appl. Opt. **43**, 4957–4964 (2004).
42. Y. Huot, A. Morel, M. S. Twardowski, D. Stramski, and R. A. Reynolds, "Particle optical backscattering along a chlorophyll gradient in the upper layer of the eastern South Pacific Ocean," Biogeosciences **5**, 495–507 (2008).
43. A. Morel, B. Gentili, H. Claustre, A. Babin, A. Bricaud, J. Ras, and F. Tieche, "Optical properties of the "clearest" natural waters," Limnol. Oceanogr. **52**, 217–229 (2007).
44. X. Zhang, L. Hu, and M.-X. He, "Scattering by pure seawater: effect of salinity," Opt. Express **17**, 5698–5710 (2009).
45. M. S. Twardowski, H. Claustre, S. A. Freeman, D. Stramski, and Y. Huot, "Optical backscattering properties of the "clearest" natural waters," Biogeosciences **4**, 1041–1058 (2007).
46. H. Loisel, J. M. Nicolas, A. Sciandra, D. Stramski, and A. Poteau, "Spectral dependency of optical backscattering by marine particles from satellite remote sensing of the global ocean," J. Geophys. Res. **111**, C09024 (2006).
47. S. Sathyendranath, L. Prieur, and A. Morel, "A three-component model of ocean colour and its application to remote sensing of phytoplankton pigments in coastal waters," Int. J. Remote Sens. **10**, 1373–1394 (1989).
48. H. R. Gordon and W. R. Mcluney, "Estimation of the depth of sunlight penetration in the sea for remote sensing," Appl. Opt. **14**, 413–416 (1975).
49. K. L. Carder, R. G. Steward, G. R. Harvey, and P. B. Ortner, "Marine humic and fulvic acids: their effects on remote sensing of ocean chlorophyll," Limnol. Oceanogr. **34**, 68–81 (1989).
50. L. Guo, P. H. Santschi, and K. W. Warnken, "Dynamics of dissolved organic carbon (DOC) in oceanic environments," Limnol. Oceanogr. **40**, 1392–1403 (1995).
51. H. R. Gordon, "Can the Lambert-Beer law be applied to the diffuse attenuation coefficient of ocean water?," Limnol. Oceanogr. **34**, 1389–1409 (1989).
52. Z. P. Lee, M. Darecki, K. L. Carder, C. Davis, D. Stramski, and W. J. Rhea, "Diffuse attenuation coefficient of downwelling irradiance: an evaluation of remote sensing methods," J. Geophys. Res. **110**, C02017 (2005).
53. A. Bricaud, M. Babin, A. Morel, and H. Claustre, "Variability in the chlorophyll-specific absorption coefficients of natural phytoplankton: analysis and parameterization," J. Geophys. Res. **100**, 13321–13332 (1995).
54. A. Bricaud, A. Morel, and L. Prieur, "Absorption by dissolved organic matter of the sea (yellow substance) in the UV and visible domains," Limnol. Oceanogr. **26**, 43–53 (1981).
55. C. S. Roesler, M. J. Perry, and K. L. Carder, "Modeling *in situ* phytoplankton absorption from total absorption spectra in productive inland marine waters," Limnol. Oceanogr. **34**, 1510–1523 (1989).
56. M. S. Twardowski, E. Boss, J. M. Sullivan, and P. L. Donaghay, "Modeling the spectral shape of absorption by chromophoric dissolved organic matter," Mar. Chem. **89**, 69–88 (2004).
57. M. J. Behrenfeld, T. K. Westberry, E. S. Boss, R. T. O'Malley, D. A. Siegel, J. D. Wiggert, B. A. Franz, C. R. McClain, G. C. Feldman, S. C. Doney, J. K. Moore, G. Dall'Olmo, A. J. Milligan, I. Lima, and N. Mahowald, "Satellite-detected fluorescence reveals global physiology of ocean phytoplankton," Biogeosciences **6**, 779–794 (2009).
58. A. Morel and S. Maritorena, "Bio-optical properties of oceanic waters: a reappraisal," J. Geophys. Res. **106**, 7163–7180 (2001).
59. J. R. V. Zaneveld., A. H. Barnard, and E. Boss, "Theoretical derivation of the depth average of remotely sensed optical parameters," Opt. Express **13**, 9052–9061 (2005).
60. Y.-J. Park and K. Ruddick, "Model of remote-sensing reflectance including bidirectional effects for case 1 and case 2 waters," Appl. Opt. **44**, 1236–1249 (2005).